Ukrainian Journal of Physical Optics
ISSUE 3
2026

STRUCTURALLY ADAPTIVE MULTILAYER RING-CORE OPTICAL FIBER FOR HYBRID OPTOELECTRONIC SENSING AND CONTROL

O. ANGELSKY [1,3], M. STRYNADKO [1], C. ZENKOVA [1], R. ZAIATS [1], ZHANG XINZHENG [2], ZHENG JUN [3]*, JINGXIAN CAI [3]

[1] Yuriy Fedkovych Chernivtsi National University, Chernivtsi, Ukraine
[2] Nankai University, Tianjin, China
[3] Taizhou Institute of Zhejiang University, Taizhou, China
* Corresponding author: dbzj@netease.com

Received: 14.12.2025

Abstract. We propose a structurally adaptive multilayer ring-core optical fiber design for hybrid optoelectronic sensing and control in compact fiber-cable links. The architecture features a protected central single-mode channel for data transmission, an auxiliary ring channel for sensing, and a programmable ring channel whose optical transmission can be electrically tuned via an adjacent conductor structure coupled to an active material region. We create a modeling workflow to evaluate channel isolation, electrode placement, and the feasibility of electrically driven actuation in the telecom band, as well as to identify practical design settings for multifunctional operation. The numerical results show that selective control of the programmable ring channel is possible while maintaining the integrity of the data backbone and sensing channel, supporting the use of such fibers as integrated tethers for robotics and distributed sensing systems.

Keywords: structurally adaptive fiber, multilayer ring-core fiber, hybrid fiber-cable, phase-change materials, electrically actuated optical conditioning, channel isolation; integrated sensing and control, robotic tether
UDC: 681.7.068
DOI: 10.3116/16091833/Ukr.J.Phys.Opt.2026.03020

1. Introduction

Optical fibers underpin modern information infrastructures, yet in most deployed systems, they remain passive waveguides that transport light between discrete active elements. A growing range of applications now motivates fibers and fiber cables that combine multiple functions - data transmission, local programmability, sensing, and power/control delivery - within a single, compact, and mechanically robust tether. This is particularly relevant for short-reach links in robotics and smart devices, where a single flexible strand is expected to provide bidirectional data exchange, distributed sensing, and electrical actuation or powering along metre-scale distances, while remaining lightweight and resistant to handling and bending.

A practical route to multifunctionality is to treat the fiber as a *family of concentric architectures* rather than a single fixed waveguide. Recent roadmaps and reviews on specialty fibers emphasize that embedding additional functionality into fibers is progressing rapidly, while manufacturability, robustness, and deployability remain central constraints for real systems [1,2]. Within this landscape, multi-ring and ring-core fibers are mature as a geometric platform for concentric multi-channel guidance within practical cladding diameters [3]. Temperature sensitivity and thermo-optic effects in ring-core geometries have also been studied, underscoring the need to manage thermal cross-effects when functional elements are introduced near guided channels [4]. These developments suggest that concentric multi-channel architectures are physically plausible — but a key question remains: can one add *electrically addressable*

programmability in a local ring channel while preserving a protected data backbone and an auxiliary sensing channel?

Phase-change materials (PCMs) offer an attractive route to non-volatile programmability in photonics. Their reversible amorphous–crystalline transitions lead to large changes in optical constants and enable persistent states without requiring static power [5]. PCM-enabled devices have advanced rapidly in photonics, supporting switching, memory, and reconfigurable signal processing with favorable energy budgets [6]. Materials development has broadened the design space towards lower-loss and broadband-transparent PCM options [7]. For a germanium–antimony–tellurium (GST) in particular, thin-film studies provide practical optical and thermal property data that can be used for physically grounded modelling of PCM–photonic interactions and heating dynamics [8]. Importantly for the fiber context, in-fiber or fiber-integrated non-volatile modulation has been demonstrated, indicating that PCM concepts can be transferred beyond planar chips [9]. Endurance and energy-efficient programming results reported for PCM photonic patches further support the feasibility from a device-engineering viewpoint [10].

A complementary enabling direction is the integration of conductors and electrodes within or around fiber structures. Prior work on fibers with embedded metal electrodes has demonstrated electrically driven actuation and Joule-heating mechanisms in fiber-compatible form factors, providing a pathway towards hybrid optoelectronic fibers [11,12]. Such approaches motivate a cable-like view: instead of a passive fiber plus external electronics, the tether itself can host both guided optical channels and concentrically arranged electrical conductors.

Beyond programmability, multifunctional fiber-cables also motivate a sensing perspective in which coherence-sensitive field structure and correlation-based diagnostics become relevant for interpreting signal behaviour in complex fiber geometries. Correlation optics and optical singularities provide a broader physical framework for coherence-aware measurement and structured-field interpretation [13,14]. Related optical-field diagnostic approaches based on correlation analysis further motivate sensing-oriented channel concepts in multifunctional fibers [15].

In this work, we develop and evaluate a structurally adaptive optical fiber-cable concept that combines these threads into a single concentric architecture. The key idea is to protect a central single-mode fiber (SMF)- like backbone channel for robust data transmission, while adding one passive ring channel (Ring-1) for sensing or auxiliary functions, and one programmable ring channel (Ring-2) whose optical attenuation can be controlled via a local PCM interaction region. Electrical actuation is provided by conductors arranged near the programmable ring (e.g., an annular electrode and an outer mesh conductor), enabling localized heating and preferential control of Ring-2 while minimizing impact on the backbone and Ring-1.

The paper's contribution is a modelling-based feasibility study of this hybrid architecture within a realistic manuscript scope. We quantify channel isolation in the presence of actuation conductors, the electrical actuation budget for representative annular versus mesh-conductor geometries, and robustness to parameter uncertainty via a compact Monte Carlo analysis targeting a specified extinction ratio. By framing the design as a family of concentric multi-channel fiber-cable architectures and analysing a representative baseline instance, the study provides quantitative guidance on how a protected backbone can coexist with a programmable ring channel in a mechanically practical tether format.

The remainder of the paper is organised as follows. Section 2 introduces the architectural family and the baseline configuration used in simulations, and summarises the governing

modelling framework. Section 3 reports the key quantitative outcomes on channel isolation, actuation feasibility, and robustness under uncertainty. Section 4 discusses the implications for multifunctional short-reach fiber cables, including practical trade-offs between conductor geometry and actuation efficiency, and outlines directions for further refinement.

2. Methods

2.1. Fiber design concept and architectural degrees of freedom

The proposed structurally adaptive fiber is formulated as a concentric fiber-cable architecture that co-integrates optical transmission, sensing, and electrically addressable optical conditioning within a single strand (Fig. 1). The concept is intentionally modular and should be regarded as a family of architectures defined by two sets of design degrees of freedom: the number and placement of guided optical channels and the number and placement of electrical conductors used for actuation and/or power delivery. Two central configurations are illustrated in Fig. 1: a conductor-centred variant (Fig. 1a) and an SMF-backbone variant used for modelling (Fig. 1b).

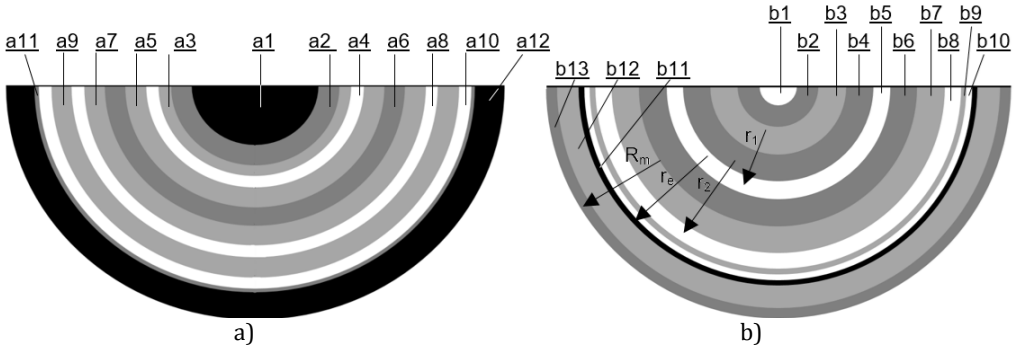

Fig. 1. Structurally adaptive fiber-cable concept and baseline architecture used for numerical evaluation.
(a) Family of concentric architectures with a central electrical conductor. The scheme illustrates a generic multilayer fiber-cable in which optical ring channels and electrical conductors are arranged concentrically around a central conductor. Layer definitions (from the centre outward): a1 – Central metallic conductor for electrical power delivery and control pulses, a2 – Electrical insulation sleeve providing dielectric isolation and thermal buffering of the conductor, a3 – Inner silica spacer ensuring optical separation between the conductor assembly and the optical backbone, a4–a6 – Ring-core single-mode backbone channel (a4 – Inner low-index cladding, a5 – Ring-core backbone guiding region, a6 – Outer cladding of the backbone channel), a7–a9 – Passive auxiliary ring channel (Ring-1) with inner cladding (a7), guiding core (a8), and outer cladding (a9), a10 – Programmable ring channel (Ring-2) intended for controlled optical conditioning, a11 – Local active-material interaction region (e.g., PCM layer stack adjacent to Ring-2), a12 – Outer dielectric jacket and/or braided-mesh conductor forming the second electrode and providing mechanical protection. This panel illustrates the flexibility of the architecture, in which the number and positions of optical rings (1…*N*) and conductors (0…*M*) can be adapted to different multifunctional fiber-cable applications.
(b) Baseline configuration analysed in this work. This configuration is used for the numerical modelling of channel selectivity and electrode placement. Layer definitions (from the centre outward): b1 – Central single-mode fiber backbone core, b2 – Backbone cladding, b3 – Mechanical/optical buffer layer protecting the backbone, b4–b6 – Passive sensing/auxiliary ring channel (Ring-1) - inner cladding (b4), guiding ring core (b5), outer cladding (b6), b7 – Inter-ring isolation layer reducing optical and thermal coupling, b8 – Programmable ring channel (Ring-2), b9 – Barrier/adhesion layer adjacent to the active region, b10 – Active-material layer (e.g., GST phase-change material), b11 – Annular electrode positioned near Ring-2 at radius r_e, b12 – Outer dielectric cladding/jacket, b13 – Outer mesh or braid conductor serving as a secondary electrode at radius r_m. The effective radii of the passive and programmable channels are denoted r_1 and r_2, respectively.

Table 1. Layer definition, candidate materials, and typical thickness (order-of-magnitude).

(a) Conductor-centred family (Fig. 1a)

Layer	Role	Candidate material(s)	Typical thickness/size
a1	Central electrical conductor	Cu, W, NiCr, stainless steel (draw-compatible choice)	Ø 10–50 μm
a2	Electrical insulation sleeve	SiO_2, polyimide, fluoropolymers (ETFE/PTFE), glass-ceramic	2–20 μm
a3	Inner silica spacer / optical buffer	Fused silica	5–50 μm
a4	Backbone inner cladding (low-index)	Fluorine-doped silica ($F–SiO_2$)	2–20 μm
a5	Backbone ring core (guiding)	Ge-doped silica ($Ge–SiO_2$)	1–8 μm
a6	Backbone outer cladding	SiO_2	5–30 μm
a7	Ring-1 inner cladding	$F–SiO_2$	2–20 μm
a8	Ring-1 core (passive)	$Ge–SiO_2$	1–8 μm
a9	Ring-1 outer cladding / buffer	SiO_2	5–40 μm
a10	Ring-2 core (programmable)	$Ge–SiO_2$ (or tailored doped silica)	1–8 μm
a11	Active interaction region adjacent to Ring-2 (stack)	Barrier: Al_2O_3/Si_3N_4; PCM: GST	Barrier 10–50 nm; PCM 50–300 nm
a12	Outer jacket/cladding (and optional mesh/braid as outer conductor)	SiO_2 jacket; optional Cu/Ni mesh	Jacket 20–200 μm; mesh layer ~10–100 μm (effective)

(b) SMF-backbone baseline (Fig. 1b)

Layer	Role	Candidate material(s)	Typical thickness/size
b1	SMF backbone core	$Ge–SiO_2$	Ø 8–10 μm *(typical SMF)*
b2	SMF backbone cladding	SiO_2	Ø 125 μm (standard) *(or scaled if multi-ring preform)*
b3	Backbone protection buffer	SiO_2/polymer buffer	5–50 μm
b4	Ring-1 inner cladding	$F–SiO_2$	2–20 μm
b5	Ring-1 core (passive)	$Ge–SiO_2$	1–8 μm
b6	Ring-1 outer cladding	SiO_2	5–40 μm
b7	Inter-ring isolation buffer	SiO_2/low-index silica	5–60 μm
b8	Ring-2 core (programmable)	$Ge–SiO_2$	1–8 μm
b9	Barrier / adhesion layer	Al_2O_3, Si_3N_4	10–50 nm
b10	PCM layer	GST (or low-loss PCM alternative)	50–300 nm
b11	Annular electrode near Ring-2	Thin metal ring: Ti/Au, NiCr, Cu (tech-dependent)	0.1–2 μm *(film)* or 2–20 μm *(wire-ring)*
b12	Outer dielectric jacket cladding	SiO_2/polymer	20–200 μm
b13	Outer mesh/braid conductor (second electrode)	Cu mesh/braid, metallised polymer braid	10–100 μm (effective)

- *The listed thicknesses are typical design ranges used for feasibility-level modelling; exact values depend on the fabrication route (stack-and-draw, deposition on preform, post-draw coating) and on the targeted balance between channel isolation, actuation efficiency, and mechanical robustness.*
- *For the PCM region, a thin barrier/adhesion layer is included to improve interface stability and to mitigate diffusion.*

2.2. Modelling framework: governing equations and boundary conditions

The modelling framework combines electromagnetic guidance analysis with compact electro-thermal feasibility estimates in a concentric multi-channel geometry. It is used to quantify channel isolation, actuation feasibility, and preferential localisation towards the programmable ring.

2.2.1. Optical formulation. In the general case, guided eigenmodes of the cross-section can be obtained in the frequency domain by solving the vector wave (eigenmode) equation for time-harmonic fields,

$$\nabla \times \left(\mu_r^{-1} \nabla \times \mathbf{E} \right) - k_0^2 \varepsilon_r \mathbf{E} = 0 \tag{1}$$

where $\boldsymbol{E}$ is the electric-field phasor, μ_r is the relative permeability, ε_r is the relative permittivity, and $k_0 = 2\pi / \lambda$ is the free-space wavenumber at wavelength λ. The permittivity is defined from the complex refractive index $\tilde{n}$ as $\varepsilon_r = \tilde{n}^2$, with $\tilde{n} = n + ik$, where n is the refractive index and k is the extinction coefficient. Material absorption and state-dependent attenuation are therefore captured through k and through changes in the modal overlap with the programmable interaction region. An absorbing outer boundary condition (e.g., a perfectly matched layer, PML) may be applied to emulate an open domain, while electromagnetic continuity is enforced at internal interfaces.

2.2.2. Compact channel-selectivity metric. To evaluate how electrode placement affects different channels without invoking a full multi-physics optimisation, we introduce a compact electrode–channel interaction proxy in which the actuation-induced optical penalty decays with the radial separation between the annular electrode radius r_e and the effective radius r_i of channel i (SMF backbone, Ring-1, Ring-2). The separation is defined as $\Delta r_i = | r_e - r_i |$, where r_e is the annular-electrode radius, and r_i is the effective radius of channel $i \in \{SMF, R1, R2\}$.

Added-loss proxy. The placement-dependent added-loss penalty (per unit length) is modelled as

$$\Delta IL_i(r_e) = \Delta IL_{i,0} \, exp\left(-\frac{\Delta r_i}{r_0} \right), \tag{2}$$

where $\Delta IL_{i,0}$ is the maximum added-loss coefficient for channel i at zero separation and r_0 is a characteristic radial decay length that sets the placement sensitivity. $\Delta IL_i(r_e)$ is interpreted as the placement-dependent additional attenuation experienced by channel *i* due to local actuation, expressed per unit length. $HLI_i(r_e)$ is a normalised indicator of how strongly the deposited heat is concentrated near channel i relative to the average across all channels.

Heat-localisation indicator. To compare how strongly actuation is localised toward the programmable channel versus the protected channels, we define a dimensionless heat-localisation indicator

$$HLI_i(r_e) = \frac{exp\left(-\frac{\Delta r_i}{r_0}\right)}{\frac{1}{3}\sum_{j\in\{SMF,R1,R2\}} exp\left(-\frac{|r_e - r_j|}{r_0}\right)}. \quad (3)$$

Here, r_e is the annular-electrode radius, r_i is the effective radius of channel i, and the index j runs over the set of channels {SMF,R1,R2}. The quantity r_j therefore denotes the effective radius of channel j in this set.

By construction, $HLI_i > 1$ indicates preferential localisation toward channel i relative to the average across channels. An annular-electrode radius sweep is then performed to map $\Delta IL_i(r_e)$ and $HLI_i(r_e)$ across the backbone and ring channels (Fig. 2), and to identify placement regions that maximise selectivity for Ring-2 while minimally affecting the SMF backbone and Ring-1.

2.2.3. Electrical actuation feasibility. Electrical feasibility is assessed using a resistive conductor model. For a conductor of electrical resistivity ρ and effective cross-sectional area A, the resistance per unit length is $R'=\rho/A$. For a prescribed drive current I and active length L, the dissipated electrical power is $P = I^2R = I^2R'L$, where $R = R'L$. Mesh or braid conductors are represented by an effective fill factor that reduces A relative to a continuous annular electrode.

2.2.4. Thermal formulation and localisation. Where required, temperature evolution can be described by the heat-diffusion equation, $\rho_m C_p \frac{\partial T}{\partial t} = \nabla\cdot(\kappa_{th}\nabla T) + Q(\mathbf{r},t)$, where $T(\mathbf{r},t)$ is temperature, ρ_m is mass density (to avoid confusion with electrical resistivity ρ), C_p is specific heat capacity, κ_{th} is thermal conductivity, and $Q(\mathbf{r},t)$ is the volumetric heat source. Joule heating in conductive domains is given by $Q=J^2/\sigma$, where σ is the electrical conductivity and $J(t)$ is the current density set by the applied electrical waveform. Thermal continuity (temperature and heat flux) is imposed at material interfaces, and the outer boundary is coupled to the ambient to emulate heat sinking. A positive localisation metric is used to compare the relative actuation impact on the backbone and ring channels; it increases with actuation power density and decreases with radial distance from the conductor to the channel.

3. Results

3.1. Channel isolation and selective actuation in the baseline architecture

We first evaluated whether the chosen actuation geometry can target the programmable ring channel (Ring-2) while leaving the protected single-mode backbone (SMF) and the auxiliary ring (Ring-1) essentially unaffected. The quantitative comparison across channels is summarised in Table 1.

The electrode-induced added loss is negligible for the SMF backbone and Ring-1 within the adopted interaction model, indicating that the protected central channel and the passive ring preserve their baseline attenuation. In contrast, Ring-2 exhibits a measurable added-loss contribution (on the order of 10^{-2}–10^{-1} dB/m), consistent with the intended programmability of this ring channel. The same baseline placement also yields the largest value of the heat-localisation metric *HLI* for Ring-2 compared with Ring-1 and the SMF

backbone, indicating preferential localisation of actuation towards the programmable ring. Together, these results support the feasibility of a *protected backbone + programmable ring* concept in a concentric fiber-cable architecture.

Table 1. Channel isolation and actuation localisation metrics for the baseline architecture (SMF backbone, Ring-1, Ring-2).

Channel	r, μm	Added loss ΔIL_{total}, dB/m	Total loss IL_{total}, dB/m	Heating localisation HLI_{total}, a.u.
SMF (backbone)	0.20	1.9×10^{-9}	0.050	0.38
Ring-1 (sensing)	20	3.7×10^{-5}	0.050	0.66
Ring-2 (programmable)	35	6.7×10^{-2}	0.12	1.9

Note. ΔIL_{total} denotes the electrode-induced added loss (optical "penalty") in the channel; IL_{total} is the total loss including the baseline contribution; HLI_{total} is the heating/actuation localisation index (the larger the value, the more strongly the actuation is localised to the given channel).

3.2. Electrode placement sweep: selectivity and localisation

To complement the baseline results and justify the choice of electrode placement, we performed a radial sweep of the annular electrode radius r_e and evaluated two compact metrics across the three channels: the actuation-induced added-loss penalty ΔIL and a heat-localisation indicator (HLI). This sweep provides a direct visual mapping of how electrode proximity preferentially affects the programmable ring channel relative to the protected backbone and the auxiliary sensing ring.

Fig. 2 shows a strong channel-dependent response as r_e is varied. The programmable channel (Ring-2) exhibits a pronounced peak in both ΔIL and HLI when the electrode is placed near its radial position, indicating preferential actuation coupling and localisation towards Ring-2.

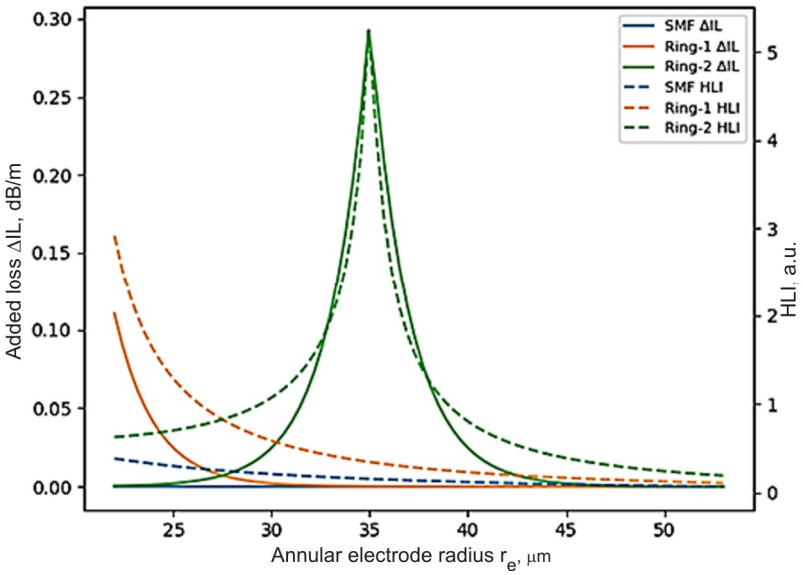

Fig. 2. Electrode placement sweep: selectivity (ΔIL) and localisation (HLI). Added-loss penalty ΔIL (left axis) and heat-localisation indicator HLI (right axis) versus annular-electrode radius r_e for the three channels (SMF backbone, Ring-1, Ring-2). Solid lines: ΔIL. Dashed lines: HLI. The sweep highlights a region of placement where the programmable Ring-2 exhibits maximal selectivity and localisation, while the backbone and Ring-1 remain weakly affected.

In contrast, the SMF backbone remains weakly affected throughout the sweep, whereas Ring-1 shows only a moderate response that decreases with increasing radial separation from the electrode.

These trends provide a clear rationale for placement: positioning the annular electrode close to Ring-2 improves selectivity while preserving the integrity of the protected backbone and the auxiliary sensing ring. Accordingly, the baseline configuration used in Tables 1–3 is chosen within the high-selectivity region indicated by Fig. 2, and the electrical budget analysis (Table 2) is reported for a representative placement in that region.

3.3. Electrical actuation budget for annular and mesh conductors

We next quantified the electrical actuation costfor the baseline configuration. The resistive budget is reported in Table 2 in terms of resistance per unit length R', power per unit length P', and total power over the active section of length L_{active}.

For the annular electrode, the computed R' is in the $\sim 10-40\,\Omega/\mathrm{m}$ range, leading to a watt-level electrical power over a 30-cm active segment at sub-ampere drive current. The mesh conductor exhibits a higher effective R' (as expected from the reduced fill factor), resulting in a higher watt-level power budget for the same actuation conditions. These results indicate that electrically driven control of a short programmable segment is feasible within practical power levels, while also highlighting the trade-off between conductor geometry (continuous annulus vs. mesh) and electrical efficiency.

3.4. Robustness to parameter uncertainty: Monte-Carlo summary for ER = 2.5 dB

To assess robustness to parameter variability and establish a practical design window, we performed a Monte Carlo analysis targeting an extinction ratio of *ER*=2.5 dB. Such an extinction ratio is sufficient for robust state discrimination in short-reach sensing or control links while remaining compatible with practical programmable-length constraints in fibre-embedded PCM segments. The target extinction ratio was set to *ER*=2.5 dB as a conservative, system-relevant threshold that is sufficiently large to enable robust state discrimination in short-reach links while remaining achievable over sub-metre programmable lengths under realistic parameter variability. The paper-ready summary (median and 5–95% interval) is provided in Table 3.

Table 2. Electrical actuation budget for the representative electrode geometries (annular electrode and mesh conductor) assuming copper conductivity, drive current I=0.60 A, and L_{active}= 0.30 m .

Conductor geometry	r ,μm	t ,μm	Fill factor	R',Ω / m	P', W / m	Total power, W
Annular electrode	38	5.0	1.0	14	5.1	1.5
Mesh electrode	55	5.0	0.25	39	14	4.2

Note. r – mean radius of the conductor (μm), t – effective conductor thickness (radial thickness for annular electrode or wire diameter equivalent for mesh strands) (μm), *fill factor* – effective conductive fill factor (dimensionless fraction of metal in the annular region; equals 1 for a solid ring, <1 for mesh/braid), R' is the resistance per unit length of the conductor, $P' = I^2 R'$ is the Joule-heating power per unit length, $P = P' L_{active}$ is the total electrical power dissipated over the active fiber length L_{active}. The parameter fill denotes the effective conductive fill factor of the annular region (1.0 for a solid ring electrode and <1 for mesh/braid geometries). All values are estimated assuming copper conductivity at room temperature.

Table 3. Monte-Carlo summary (median and 5–95% interval) for the *ER* = 2.5 dB target: IL_{ON}, off-state attenuation (per 10 cm), and required active length.

Quantity	Median	5%	95%	Units
IL_{ON}	0.35	0.33	0.37	dB/m
OFF-state attenuation	0.51	0.44	0.58	dB/10 cm
Required active length for *ER* = 2.5 dB	52.70	45.41	61.32	cm

The results indicate that the on-state attenuation IL_{ON} remains within a narrow band across the evaluated uncertainty range, whereas the off-state attenuation expressed per 10-cm segment shows a broader spread. In terms of system-level implication, achieving *ER*=2.5 dB requires an active length on the order of 0.5 m under the analysed uncertainty model. For a shorter baseline segment (e.g., 20 cm), the attainable extinction ratio remains below the 2.5 dB target, implying that either a longer active section or a stronger programmable interaction is required to meet the chosen *ER* specification.

3.5. Dominant sensitivity factors (compact ranking)

A compact sensitivity ranking provides further guidance on which parameters most strongly influence performance. The on-state attenuation is dominated by scattering/roughness-related terms, whereas *ER*-related metrics (off-state attenuation and required active length) are primarily governed by programmable-interaction parameters (e.g., the effective interaction factor and PCM-related strength terms). This separation is practically useful: on-state loss is primarily governed by fabrication-quality terms (surface/interface losses), while extinction and required length are determined by the programmable coupling strength and its tolerances.

4. Discussion

This work was motivated by the need for compact, mechanically practical fiber-cable links that combine robust data transport with local programmability and auxiliary sensing. Rather than pursuing extreme nonlinearity or complex external modulation hardware, we framed the design as a concentric *family* of architectures and evaluated a representative baseline instance with a protected SMF-like backbone channel, a passive auxiliary ring (Ring-1), and a programmable ring (Ring-2) addressed by nearby conductors. Absolute values depend on specific material parameters and fabrication tolerances, while the presented modelling highlights design trends and feasible operating windows.

4.1. Key implication: protected backbone with a selectively addressable ring channel

A central question for hybrid optoelectronic fibers is whether electrical actuation structures can be positioned sufficiently close to the active ring to enable meaningful control without degrading neighbouring optical channels. The modelling results indicate that this requirement can be met in a multilayer concentric architecture. In particular, the spatial separation between the protected backbone channel and the programmable ring allows actuation effects to be localised primarily within the selected ring region while leaving the central data path largely unaffected.

This observation has an important architectural implication. It confirms that a concentric multilayer fiber can support functional partitioning between transmission, sensing, and control. The central SMF backbone can be treated as a stable infrastructure channel for data transfer or reference sensing, while an outer programmable ring can implement electrically controlled

attenuation or phase conditioning. Additional rings may serve auxiliary sensing or monitoring roles without requiring the same degree of electrical coupling. Such segregation is difficult to achieve in single-core or uniformly doped fibers, where any active material or electrode placement directly perturbs the primary guided mode.

From an engineering standpoint, selective programmability enables several practical functions within a single fiber strand. These include adaptive attenuation or weighting of signals, state-dependent routing in short fiber links, distributed threshold sensing, and local reconfiguration of optical paths in robotic or embedded systems. Because the data backbone remains protected, these functions can be introduced without compromising communication reliability, which is critical for compact multifunctional tethers.

The results also suggest that conductor placement is a key design parameter rather than a fixed structural choice. By adjusting the radial position and geometry of electrodes, one can tune the balance between programmability and channel isolation. This flexibility allows the same general fiber concept to be adapted for different applications—for example, stronger coupling for switching-oriented devices or weaker coupling for sensing-dominated configurations.

Overall, the modelling supports the feasibility of combining a protected optical backbone with selectively addressable ring channels in a single multilayer fiber. This capability provides a physical basis for multifunctional fiber-cable links in which transmission, sensing, and control coexist within one mechanically robust structure, opening opportunities for integrated photonic tethers in robotics, distributed sensing networks, and compact optoelectronic systems.

4.2. Conductor geometry trade-off: annular electrode versus mesh conductor

The electrical analysis reveals a practical trade-off between actuation efficiency and structural flexibility. A continuous annular electrode provides a lower resistance per unit length $R' = \rho / A$ and therefore requires less electrical power to achieve a given thermal load in the programmable region for a prescribed current and active length. This configuration is advantageous when minimising drive current, heating losses, or overall power consumption is the dominant design objective, for example, in battery-powered robotic tethers or compact distributed sensor nodes.

In contrast, mesh or braided conductor geometries offer benefits that can be equally important in realistic fiber-cable implementations. Such structures improve mechanical compliance, tolerate bending and vibration more effectively, and can simultaneously serve as electromagnetic shielding layers. They are also compatible with standard hybrid cable technologies that routinely use conductive braids for protection and grounding. These advantages are achieved at the cost of increased effective resistance, which can be represented in the modelling framework by a reduced conductive fill factor (f<1), leading to higher dissipated power under the same drive conditions.

From a system-design perspective, the annular and mesh conductors represent limiting cases within a broader design space. The optimal solution depends on the dominant constraint of the intended application – energy efficiency, mechanical robustness, manufacturability, or electromagnetic compatibility. Regardless of geometry, the critical requirement remains that the conductor placement is preferentially coupled to the programmable ring channel while preserving the optical integrity of the protected backbone and auxiliary rings.

This interpretation highlights that conductor geometry is not merely a mechanical detail but a co-design parameter linking electrical, thermal, and optical performance in structurally adaptive fiber systems.

4.3. Robustness and design targets inferred from Monte-Carlo analysis

The Monte-Carlo analysis provides a system-level interpretation of how fabrication and material variability propagate into performance metrics of the proposed fiber architecture. Within the adopted uncertainty model, the on-state attenuation of the backbone channel remains comparatively stable, whereas the off-state attenuation and the active length required to achieve a target extinction ratio are more sensitive to parameters governing the programmable interaction region.

This behaviour indicates that short programmable sections may not reliably satisfy stronger extinction-ratio specifications under realistic tolerances, while longer active segments provide a safety margin against parameter spread. In practical terms, the target extinction ratio should therefore be selected jointly with the available programmable length and the achievable interaction strength between the electrode and the active-material region.

The compact sensitivity ranking further separates fabrication-dominated and programmability-dominated factors. Parameters associated with scattering losses, surface roughness, and baseline material absorption primarily determine the on-state insertion loss. In contrast, the extinction-ratio performance is dominated by parameters controlling modal overlap with the programmable ring, PCM optical constants, and electrode placement. This separation suggests a staged optimisation strategy: first minimise baseline losses through fabrication-quality control, and then tune programmability through interaction strength, conductor geometry, and electrode position.

Overall, the Monte-Carlo results confirm that the proposed architecture admits practical design windows in which channel isolation and programmable contrast can be achieved simultaneously under realistic parameter variability.

4.4. Scope, limitations, and next steps

The present study is intentionally modelling-focused and addresses feasibility-level questions within a constrained manuscript scope. Compact metrics – such as the actuation-induced added-loss penalty and the heat-localisation indicator – were used as proxies to compare channel responses and conductor placements without performing a full multi-physics optimisation across all possible ring configurations.

Similarly, the analysed baseline configuration represents one instance within a broader family of structurally adaptive fiber-cable architectures. Alternative layouts, including different numbers of ring channels, multiple conductors, or conductors placed in other radial zones, are compatible with the same modelling framework and may be preferable under specific mechanical, thermal, or manufacturability constraints.

Future work should therefore extend modelling fidelity where necessary, for example, through fully coupled eigenmode and electro-thermal simulations for selected geometries, and through experimental validation of material parameters, boundary conditions, and switching dynamics in prototype fiber segments. In particular, measurements of insertion loss, extinction ratio, thermal localisation, and endurance will be important for refining the model parameters and confirming achievable operating windows.

Despite these limitations, the current results already provide actionable guidance for system design. They show that a protected central backbone can coexist with a selectively

addressable programmable ring channel, and that the required actuation power can be brought into a practical range through appropriate conductor geometry and placement. These conclusions support the viability of structurally adaptive multilayer fibers as multifunctional tethers for distributed sensing, hybrid optoelectronic links, and compact robotic systems.

5. Conclusion

We presented a modelling-based feasibility study of a structurally adaptive multilayer ring-core fiber-cable architecture designed for hybrid optoelectronic sensing and control. The concept treats the design as a family of multi-channel architectures and evaluates a representative baseline configuration consisting of a protected SMF-like backbone channel for robust data transmission, a passive auxiliary ring channel (Ring-1), and a programmable ring channel (Ring-2) coupled to a local phase-change material interaction region and addressed by nearby conductors.

Numerical eigenmode and electro-thermal modelling results support three main conclusions. First, the baseline architecture enables effective functional separation: actuation structures can preferentially address Ring-2 while incurring negligible additional loss in the backbone and Ring-1 channels over the explored parameter range. Second, a practical electrical actuation budget is achievable over short active lengths, with a clear trade-off between continuous annular electrodes and mesh conductors in terms of efficiency versus mechanical flexibility. Third, a compact Monte-Carlo uncertainty analysis shows that achieving a specified extinction ratio requires sufficient programmable length and interaction strength, and it identifies the dominant sensitivity factors governing on-state insertion loss versus ER-related performance.

Overall, the study provides quantitative design guidance for compact, multifunctional fiber-optic cables in short-reach applications, including robotic tethers and distributed-sensing links. By demonstrating the feasibility of a protected backbone coexisting with a selectively addressable programmable ring channel in a multilayer ring-core structure, the proposed framework outlines a practical pathway towards mechanically robust hybrid optoelectronic fiber-cable systems with integrated in-fiber programmability and sensing capabilities.

Funding and acknowledgments. This research was supported by the Department of Correlation Optics at Yuriy Fedkovych Chernivtsi National University, and by the National Research Foundation of Ukraine (NRFU) under project No. 2025.07/0069 “Recent applications of structured optical fields in polarization-interference methods for solving problems in telecommunications, and biomedicine” and project No. 2025.06/0086 “Innovative Methods and Systems of Laser Communication in Turbulent Atmospheric Environments Based on Phase Singularities”.

The authors gratefully acknowledge financial support from the Taizhou Institute of Zhejiang University in Taizhou, China, for the open-access publication.

Disclosures. The authors declare no conflict of interest.

Authors contribution. O. Angelsky: Project administration, resources, supervision, validation. M. Strynadko: Conceptualization, data curation, formal analysis, investigation, methodology, visualization, writing – original draft. C. Zenkova, R. Zaiats, Xinzheng Zhang, Jun Zheng, Jingxian Cai: validation, writing – review & editing.

References

1. Ferreira, M. F., Rehan, M., Mishra, V., Varshney, S. K., Poletti, F., Phuoc Trung Hoa, N., ... & Reitzenstein, S. (2025). Roadmap on specialty optical fibers. *Journal of Physics: Photonics*, *7*(1), 012501.
2. Schuster, K., Unger, S., Aichele, C., Lindner, F., Grimm, S., Litzkendorf, D., Kobelke, J., Bierlich, J., Wondraczek, K., & Bartelt, H. (2014). Material and technology trends in fiber optics. *Advanced Optical Technologies*, *3*(4), 447-468.
3. Li, S., & Wang, J. (2014). A compact trench-assisted multi-orbital-angular-momentum multi-ring fiber for ultrahigh-density space-division multiplexing (19 rings× 22 modes). *Scientific reports*, *4*(1), 3853.
4. Vigneswaran, D., Mani Rajan, M. S., Aly, M. H., & Rashed, A. N. Z. (2019). Few-mode ring core fiber characteristics: temperature impact. *Photonic Network Communications*, *37*(1), 131-138.
5. Wuttig, M., & Yamada, N. (2007). Phase-change materials for rewriteable data storage. *Nature Materials*, *6*(11), 824-832.
6. Zhou, W., Farmakidis, N., Feldmann, J., Li, X., Tan, J., He, Y., Wright, C. D., Pernice, W. H. P., & Bhaskaran, H. (2022). Phase-change materials for energy-efficient photonic memory and computing. *MRS Bulletin*, *47*(5), 502-510.
7. Zhang, Y., Chou, J. B., Li, J., Li, H., Du, Q., Yadav, A., ... & Hu, J. (2019). Broadband transparent optical phase change materials for high-performance nonvolatile photonics. *Nature communications*, *10*(1), 4279.
8. Aryana, K., Kim, H. J., Islam, R., Hong, N., Popescu, C.-C., Makarem, S., Gu, T., Hu, J., Hopkins, P.E. (2023). Optical and thermal properties of $Ge_2Sb_2Te_5$ thin films for photonic devices. *Optical Materials Express*, *13*, 3277–3291.
9. Liu, Z., Li, X., Cheng, S., Li, Y., Jin, W., Zhang, Y., Li, S., Lotnyk, A., & Yuan, L. (2023). All-optical nonvolatile optical modulator for in-fiber operation. *Nanophotonics*, *12*(15), 3179-3187.
10. Sawant, R., Albanese, A., Rogemont, A., Gonzalez-Cortes, G., Brûlé, Y., Karam, L., Jager J.-B., Malhouitre S., Charbonnier B., Coillet A., Noé P., & Cluzel, B. (2025). High-Endurance and Energy-Efficient All-Optical Programming of Scalable Silicon Waveguides with Integrated Phase-Change Material Patches. *Advanced Optical Materials*, *13*(25), e00775.
11. Lian, Z., Segura, M., Podoliak, N., Feng, X., White, N., Horak, P., & Loh, W. H. (2014, March). Electrical current-driven dual-core optical fiber with embedded metal electrodes. In *Optical Fiber Communication Conference* (pp. Tu3K-3). Optica Publishing Group.
12. Lian, Z., Segura, M., Podoliak, N., Feng, X., White, N., & Horak, P. (2014). Nanomechanical optical fiber with embedded electrodes actuated by joule heating. *Materials*, *7*(8), 5591-5602.
13. Angelsky, O. V., Bekshaev, A. Y., Zenkova, C. Y., Ivansky, D. I., & Zheng, J. (2022). Correlation optics, coherence and optical singularities: Basic concepts and practical applications. *Frontiers in Physics*, *10*, 924508.
14. Angelsky, O. V., Bekshaev, A. Y., Vasnetsov, M. V., Zenkova, C. Y., Maksimyak, P. P., & Zheng, J. (2022). Optical phase singularities: Physical nature, manifestations and applications. *Frontiers in Physics*, *10*, 1060787.
15. Angelsky, O. V., Zenkova, C. Y., Hanson, S. G., Ivansky, D. I., Tkachuk, V. M., & Zheng, J. (2021). Random object optical field diagnostics by using carbon nanoparticles. *Optics Express*, *29*(2), 916-928.

Angelsky, O., Strynadko, M., Zenkova, C., Zaiats, R., Xinzheng, Zh., Jun, Zh., Cai, J. (2026). Structurally Adaptive Multilayer Ring-Core Optical Fiber for Hybrid Optoelectronic Sensing and Control. *Ukrainian Journal of Physical Optics*, *27*(3), 03020 – 03032.
doi: 0.3116/16091833/Ukr.J.Phys.Opt.2026.03020

Анотація. *У роботі запропоновано концепцію структурно-адаптивного багатошарового оптичного волокна з кільцевими каналами для гібридних оптоелектронних задач сенсорики та керування у компактних волоконно-кабельних лініях. Архітектура поєднує захищений центральний одномодовий канал для передавання даних, допоміжний кільцевий канал для сенсорики та програмований кільцевий канал, оптичне пропускання якого можна електрично регулювати завдяки провідниковій структурі, розташованій поблизу цього кільця та поєднаній з активною областю матеріалу. Розроблено модельний підхід для оцінювання ізоляції каналів, чутливості до розміщення електродів і можливості електричного збудження в телекомунікаційному діапазоні, а також для визначення практичних конструкційних меж багатофункціональної роботи. Чисельні результати вказують на можливість селективного керування програмованим кільцевим каналом зі збереженням цілісності каналу передачі даних і сенсорного каналу, що обґрунтовує використання таких волокон, як інтегрованих тросів для робототехніки та розподілених сенсорних систем.*

Ключові слова: *структурно-адаптивне волокно, багатошарове волокно з кільцевою серцевиною, гібридний волоконно-кабельний зв'язок, фазозмінні матеріали, електрично кероване оптичне кондиціювання, ізоляція каналів, інтегрована сенсорика та керування, робототехнічний трос*